
ARE YOU **SURE**? ENHANCING MULTIMODAL PRE-TRAINING WITH MISSING MODALITIES THROUGH UNCERTAINTY ESTIMATION

Duy A. Nguyen

Siebel School of Computing and Data Science
University of Illinois, Urbana-Champaign
Illinois, USA
duyan2@illinois.edu

Quan Huu Do

College of Engineering and Computer Science
VinUniversity
Hanoi, Vietnam
quan.dh@vinuni.edu.vn

Khoa D. Doan

College of Engineering and Computer Science
VinUniversity
Hanoi, Vietnam
khoa.dd@vinuni.edu.vn

Minh N. Do

Department of Electrical and Computer Engineering
University of Illinois, Urbana-Champaign
Illinois, USA
minhdo@illinois.edu

ABSTRACT

Multimodal learning has demonstrated incredible successes by integrating diverse data sources, yet it often relies on the availability of all modalities - an assumption that rarely holds in real-world applications. Pretrained multimodal models, while effective, struggle when confronted with small-scale and incomplete datasets (i.e., missing modalities), limiting their practical applicability. Previous studies on reconstructing missing modalities have overlooked the reconstruction's potential unreliability, which could compromise the quality of the final outputs. We present **SURE** (Scalable Uncertainty and Reconstruction Estimation), a novel framework that extends the capabilities of pretrained multimodal models by introducing latent space reconstruction and uncertainty estimation for both reconstructed modalities and downstream tasks. Our method is architecture-agnostic, reconstructs missing modalities, and delivers reliable uncertainty estimates, improving both interpretability and performance. SURE introduces a unique Pearson Correlation-based loss and applies statistical error propagation in deep networks for the first time, allowing precise quantification of uncertainties from missing data and model predictions. Extensive experiments across tasks such as sentiment analysis, genre classification, and action recognition show that SURE consistently achieves state-of-the-art performance, ensuring robust predictions even in the presence of incomplete data.

1 INTRODUCTION

Motivation. Multimodal learning has emerged as a powerful paradigm for processing raw data from diverse sources and formats, frequently outperforming unimodal approaches Huang et al. (2021). While these frameworks achieve state-of-the-art performance across numerous tasks Zong & Sun (2023); Wan et al. (2023); Wu et al. (2024), their success often hinges on idealized conditions during training and evaluation, assuming access to complete modalities and large-scale datasets. In real-world settings, such as autonomous vehicles or medical centers, these ideal conditions are rarely met due to incomplete or noisy data.

To tackle data bottleneck with small-scaled datasets, leveraging pretrained models has proven highly effective in unimodal learning He et al. (2016); Devlin (2018). This approach, however, remains underexplored in multimodal contexts. To demonstrate its potential, we evaluated a state-of-the-art multimodal fusion model, MMML Wu et al. (2024), on the CMU-MOSI dataset Zadeh et al. (2016). Two versions of the model were compared: one initialized with pretrained weights from

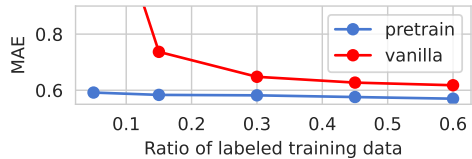


Figure 1: Comparison of pretrained and vanilla MMML framework on CMU-MOSI dataset.

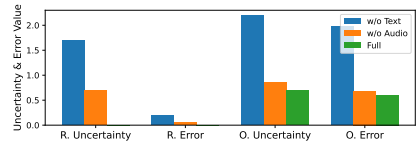


Figure 2: SURE reconstructs missing modalities for final predictions, reporting average errors and uncertainties for both reconstruction (R.) and output (O.).

the larger CMU-MOSEI dataset Zadeh et al. (2018) and another trained from scratch (i.e. vanilla). Performance was assessed across varying dataset sizes (Figure 1), revealing the clear advantages of pretrained models in terms of both efficiency and effectiveness on small-scale datasets.

A significant challenge, however, lies in the inability of pretrained multimodal frameworks to handle missing modalities (i.e. some samples come with incomplete sets of multimodal inputs) during training or evaluation. While various reconstruction techniques can impute the missing modalities, these methods alone fail to address the critical issue of prediction reliability under such conditions. Incorporating uncertainty estimation, therefore, becomes essential—not only for quantifying the reliability of predictions but also for making informed decisions in scenarios where safety and trustworthiness are paramount (e.g., healthcare and autonomous driving).

To highlight the importance of uncertainty estimation, we conducted experiments on the CMU-MOSI evaluation dataset under various modality-missing conditions. A simple reconstruction mechanism was used to approximate missing modalities, and the model’s performance was evaluated using both Mean Squared Error (MSE) and Estimated Uncertainty (Figure 2). The results showed that while missing modalities degrade performance (especially when text is absent), the model generates meaningful uncertainty estimates that align with its prediction errors. Higher average uncertainties consistently correspond to higher errors, demonstrating the utility of uncertainty estimation as a proxy for prediction reliability in multimodal settings.

Current Literature. The challenge of missing modalities is a common issue in the training and deployment of multimodal models. Research has primarily addressed this through three approaches: (1) Contrastive loss-based methods, which align latent spaces for cross-modal knowledge transfer Ma et al. (2022); Li et al. (2024b;a); (2) Generative approaches, including VAE-based models Wu & Goodman (2018) and latent space reconstruction Woo et al. (2023); Lian et al. (2023), to approximate missing modalities; and (3) Prompt-based techniques, which utilize trainable prompts to adapt models to various combinations of missing modalities Lee et al. (2023); Jang et al. (2024). The latter two approaches offer practical solutions for addressing missing modalities and are particularly effective when integrated with pretrained multimodal frameworks. These methods bridge the gap left by missing modalities without requiring extensive modifications to the pretrained models, enabling efficient adaptation to real-world scenarios. However, they overlook the critical need to quantify the uncertainty of reconstructed inputs – an essential factor for ensuring reliable downstream predictions.

A growing body of research addresses the second challenge: assessing prediction reliability through uncertainty estimation. Key methods include Bayesian deep learning Wang et al. (2019b); Kendall & Gal (2017a), which models uncertainty directly via output distributions, and post-hoc techniques like Deep Ensembles Lakshminarayanan et al. (2017), which introduce input perturbations to generate multiple predictions for uncertainty estimation. Adapting such approaches for multimodal settings, particularly in conjunction with pretrained frameworks and reconstruction techniques, provides a pathway to more robust and uncertainty-aware models. A more comprehensive review of related works is provided in Appendix A.1.

Our approach. To tackle real-world scenarios with small-scale datasets and missing modalities, we leverage pretrained multimodal frameworks augmented by a simple latent space reconstruction strategy. However, the primary focus of this work is emphasizing the critical need for uncertainty estimation as a central framework enhancement, addressing the challenge of robust multimodal learning in the presence of incomplete data, especially in applications involving *pretrained* multimodal

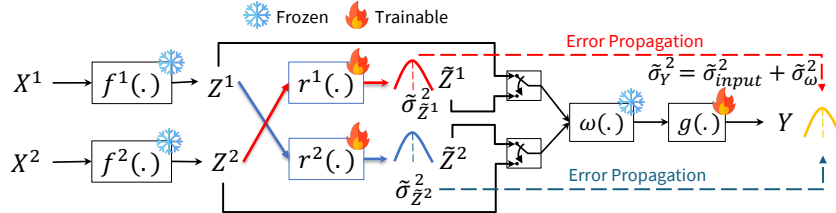


Figure 3: Overview of SURE. Reconstruction modules $r^i(\cdot)$ are inserted after latent projections $f^i(\cdot)$ and before fusion layers $\omega(\cdot)$ in pretrained multimodal frameworks, reconstructing missing modalities with uncertainties. Reconstructed outputs replace missing inputs while propagating uncertainty, and the final classifier estimates output uncertainty from the model’s inherent variability. The notation $\tilde{\bullet}$ distinguishes SURE trainable modules’ estimates from inputs, outputs, and frozen module’s intermediate variables.

models. We analyze the uncertainties associated with both the reconstruction process of missing modalities and the model’s outputs, emphasizing their interdependence and impact on downstream task performance. Specifically, higher reconstruction uncertainty often correlates with higher output uncertainty, which results in greater prediction error (Figure 2). To achieve this, three types of uncertainties are investigated:

- (1) Reconstruction uncertainty for missing modalities.
- (2) Output uncertainty due to reconstructed inputs.
- (3) Output uncertainty inherent to the model’s nature.

For effective learning of reconstruction uncertainty (1) and aggregated output uncertainty (2 + 3), we introduce a novel loss function based on Pearson Correlation, designed to balance task-specific optimization with uncertainty estimation (Section 2.2). To quantify output uncertainty stemming from reconstructed inputs (2), we adapt Error Propagation Arras (1998); Tellinghuisen (2001) for use in deep neural network training, enabling the model to effectively propagate uncertainty from reconstructed inputs to final predictions (Section 2.3). The resulting framework, named SURE (Scalable Uncertainty and Reconstruction Estimation), integrates seamlessly with pretrained multimodal models, providing a scalable and efficient solution for handling missing modalities while generating robust uncertainty estimates. By enabling the model to recognize uncertain predictions and respond with “I am not sure” when appropriate, SURE enhances reliability in safety-critical applications. In summary, our key contributions include:

- Investigation of the interdependence between reconstruction uncertainty, output reliability, and downstream task performance.
- Novel loss function to estimate uncertainty of multimodal models; first adaptation of Error Propagation for Deep Networks.
- State-of-the-art results on multiple downstream tasks with accurate uncertainty estimation mechanisms.

2 PROPOSED METHOD

We propose SURE, a framework designed to handle small-scale datasets with missing modalities by effectively estimating and leveraging uncertainty. Let $D = \bigcup_i \{(\mathbf{x}_i, \mathbf{y}_i)\}$ be the training set with pairs from domain $\mathcal{X} = \mathbb{R}^{n_1} \times \dots \times \mathbb{R}^{n_M}$ and $\mathcal{Y} = \mathbb{R}^k$. Let denote $\mathbf{x}_i = (\mathbf{x}_i^1, \dots, \mathbf{x}_i^M)$ is the i^{th} input sample where \mathbf{x}_i^j is its j^{th} modality. We address scenarios where certain modalities are missing during training or evaluation, requiring the model to operate reliably despite incomplete inputs. The following sections describe our approach to reconstruct missing modalities and estimate uncertainty in such settings.

2.1 OVERVIEW OF SURE FRAMEWORK

The proposed pipeline is shown in Figure 3. For simplicity, we illustrate the SURE pipeline with two modalities, with its extension to M modalities detailed in Appendix A.2.3. Only the reconstruction modules $r^i(\cdot)$, tailored for each modality, and the final classifier head $g(\cdot)$ require training. This design preserves most of the pretrained framework, except for the final classifier head, consistent with standard unimodal pretraining and fine-tuning procedures. In this study, we preserve the downstream functionality of pretrained frameworks by reconstructing missing modalities while **prioritizing the reliability of final predictions**, which is the core objective of SURE.

For the first objective, SURE introduces an efficient reconstruction procedure within the shared latent space. Let Z^i denote the latent representation for the i^{th} modality produced by the pretrained framework’s unimodal projectors ($f^i(\cdot)$ in Fig.3). To reconstruct a missing modality, SURE incorporates reconstruction modules $r^i(\cdot)$, each designed specifically for a particular modality. The reconstructor for the i^{th} modality, $r^i(\cdot)$, utilizes the latent representation of another available modality (e.g., Z^j) to generate an approximation \tilde{Z}^i when the i^{th} modality is missing, such that $r^i(Z^j) = \tilde{Z}^i$ ($i = 1, \dots, M; j \neq i$). While these modules are simple and efficient, their primary role is to ensure input completeness for downstream tasks. Additional design details and analysis are discussed in Appendix A.2.2.

The second and more critical objective is to quantify the reliability of both reconstructed inputs and final predictions. To achieve this, SURE designs the reconstruction modules and classifier head to not only generate outputs but also estimate their corresponding uncertainties. Specifically, the reconstruction module $r^i(\cdot)$ provides an estimate of the i^{th} modality representation \tilde{Z}^i along with its reconstruction uncertainty. Similarly, the classifier head makes final predictions while simultaneously capturing the prediction uncertainty arising from the model’s stochastic nature. Since reconstructed inputs (e.g., \tilde{Z}^i) inherently introduce uncertainty into the output, we extend the analysis of output uncertainty by quantifying how reconstruction uncertainty propagates through the entire model. This is achieved using a tailored adaptation of error propagation techniques (Section 2.3). To effectively learn uncertainty estimates, we introduce a novel distribution-free loss function (Section 2.2), which circumvents the limitations of conventional approaches and provides a more flexible measure of uncertainty.

Emphasizing uncertainty estimation as the core innovation, SURE ensures robust and interpretable predictions even in scenarios with incomplete data, while latent reconstruction serves as a straightforward but necessary step to leverage pretrained frameworks for downstream tasks.

2.2 DISTRIBUTION-FREE UNCERTAINTY ESTIMATION

Problem Formulation. Uncertainty estimation aims to quantify the reliability of model predictions, particularly in our case - scenarios with incomplete data (missing modalities). Given an incomplete input $x_i \in \mathcal{X}$, a model ϕ with parameters θ predicts an output \tilde{y}_i along with an associated uncertainty estimate $\tilde{\sigma}_i^2$. The goal is to ensure that $\tilde{\sigma}_i^2$ effectively reflects the true prediction error, e.g. $\tilde{\sigma}_i^2 \approx \|\tilde{y}_i - y_i\|^2$, where y_i is the corresponding groundtruth.

Conventional Approach. A common approach to uncertainty modeling is optimizing network parameters to estimate $\mathcal{P}_{\mathbf{Y}|\mathbf{X}}$, often chosen for its closed-form uncertainty estimation. A common choice for $\mathcal{P}_{\mathbf{Y}|\mathbf{X}}$ is the heteroscedastic Gaussian Upadhyay et al. (2022); Kendall & Gal (2017c), where the model learns both a mean prediction \tilde{y}_i and variance $\tilde{\sigma}_i^2$ as parameters of a Gaussian distribution: $\{\tilde{y}_i, \tilde{\sigma}_i\} := \phi(\mathbf{x}_i; \theta)$. To estimate these parameters, the standard approach maximizes the likelihood:

$$\theta^* = \operatorname{argmax}_{\theta} \prod_{i=1}^N \frac{1}{\sqrt{2\pi\tilde{\sigma}_i^2}} \exp\left(-\frac{\|\tilde{y}_i - y_i\|^2}{2\tilde{\sigma}_i^2}\right), \quad (1)$$

which is equivalent to minimizing NLL loss:

$$\mathcal{L}_{NLL} = \sum_{i=1}^N \frac{\|\tilde{\mathbf{y}}_i - \mathbf{y}_i\|^2}{2\tilde{\sigma}_i^2} + \frac{\log(\tilde{\sigma}_i^2)}{2}. \quad (2)$$

From this formulation, the uncertainty estimate follows:

$$\tilde{\sigma}_i^{2*} = \|\tilde{\mathbf{y}}_i - \mathbf{y}_i\|^2 = \tilde{\epsilon}_i^2. \quad (3)$$

Limitations of NLL Loss. Despite its widespread use, NLL loss has several key limitations:

- **Assumption of output distribution** – The method assumes $\mathcal{P}_{\mathbf{Y}|\mathbf{X}}$ follows a particular distribution (e.g. Gaussian), which may not hold in real-world scenarios, leading to unreliable uncertainty estimates.
- **Ill-defined Gradients for Low Errors** – When prediction error $\tilde{\epsilon}^2 \rightarrow 0$, the gradient of \mathcal{L}_{NLL} is ill-defined, causing trouble to effectively learn uncertainty (detailed analysis in Appendix A.2.1).
- **Magnitude Constraint** – The model is constrained to scale uncertainty $\tilde{\epsilon}^2$ directly with error ϵ^2 , rather than learning a flexible, robust confidence measure. Ideally, uncertainty should reflect confidence independently of error magnitude.

Our method. To circumvent these limitations, we propose a distribution-free loss function that enforces a strong correlation between uncertainty estimates and actual prediction error, without restrictive magnitude constraints. We achieve this by leveraging the Pearson Correlation Coefficient (PCC):

$$\mathcal{L}_{PCC}(\tilde{\sigma}^2, \tilde{\epsilon}^2) = 1 - r(\tilde{\sigma}^2, \tilde{\epsilon}^2), \quad \text{where} \quad (4)$$

$$r(\tilde{\sigma}^2, \tilde{\epsilon}^2) = \frac{\sum_{i=1}^N (\tilde{\sigma}_i^2 - \mu_{\sigma^2})(\tilde{\epsilon}_i^2 - \mu_{\epsilon^2})}{\sqrt{\sum_{i=1}^N (\tilde{\sigma}_i^2 - \mu_{\sigma^2})^2} \sqrt{\sum_{i=1}^N (\tilde{\epsilon}_i^2 - \mu_{\epsilon^2})^2}}. \quad (5)$$

Here, μ_{σ^2} and μ_{ϵ^2} are the means of $\tilde{\sigma}^2$ and $\tilde{\epsilon}^2$, respectively. Since Pearson correlation normalizes covariance, the loss is bounded between 0 and 2. A value of 0 indicates perfect alignment between uncertainty $\tilde{\sigma}^2$ and error $\tilde{\epsilon}^2$, while higher values imply weaker or inverse relationships.

Theorem 2.1. Let $\tilde{\sigma}_i^2$ and $\tilde{\epsilon}_i^2$ be the standardized uncertainty and squared error within a mini-batch: $\tilde{\sigma}_i^2 = \frac{\tilde{\sigma}_i^2 - \mu_{\sigma^2}}{\sqrt{\frac{1}{N-1} \sum_{j=1}^N (\tilde{\sigma}_j^2 - \mu_{\sigma^2})^2}}$, $\tilde{\epsilon}_i^2 = \frac{\tilde{\epsilon}_i^2 - \mu_{\epsilon^2}}{\sqrt{\frac{1}{N-1} \sum_{j=1}^N (\tilde{\epsilon}_j^2 - \mu_{\epsilon^2})^2}}$. Then, \mathcal{L}_{PCC} is approximately equivalent to the MSE between standardized uncertainty and error:

$$\frac{1}{2N} \sum_{i=1}^N (\tilde{\sigma}_i^2 - \tilde{\epsilon}_i^2)^2 \approx \mathcal{L}_{PCC}(\tilde{\sigma}^2, \tilde{\epsilon}^2). \quad (6)$$

Proof. Expanding the LHS:

$$\begin{aligned} \frac{1}{2N} \sum_{i=1}^N (\tilde{\sigma}_i^2 - \tilde{\epsilon}_i^2)^2 &= \frac{1}{2N} \left((2N-2) - 2 \sum_{i=1}^N \tilde{\sigma}_i^2 \tilde{\epsilon}_i^2 \right) \\ &= \frac{2N-2}{2N} (1 - r(\tilde{\sigma}^2, \tilde{\epsilon}^2)) \approx \mathcal{L}_{PCC}. \end{aligned}$$

□

Key Implications. Unlike NLL loss, which rigidly forces uncertainty to scale with error, PCC loss enables a more flexible learning of uncertainty while preserving its correlation with error. This relaxed constraint ensures that uncertainty remains a meaningful confidence indicator—predictions with higher uncertainty generally correspond to higher errors, while lower uncertainty is associated with more reliable predictions. Additionally, we later show in Appendix A.2.1 that our loss function

prevents miscalibrated uncertainty in low-error cases by promoting a more stable training process near the optimal solution, which is not the case for ordinary Gaussian NLL loss.

Integration with SURE’s Training Objectives. While \mathcal{L}_{PCC} serves as the core loss for uncertainty estimation, additional loss functions guide reconstruction and downstream task learning. For instance, final loss guiding SURE’s reconstruction modules is:

$$\mathcal{L}_{rec}^i(\tilde{\mathbf{z}}^i, \tilde{\sigma}_{z^i}^2) = \frac{1}{N} \sum \|\tilde{\mathbf{z}}^i - \mathbf{z}^i\|^2 + \lambda \cdot \mathcal{L}_{PCC}(\tilde{\sigma}_{z^i}^2, \tilde{\epsilon}^2). \quad (7)$$

Here, the MSE term guides the learning of reconstructed $\tilde{\mathbf{z}}^i$, while \mathcal{L}_{PCC} ensures σ^2 accurately reflects reconstruction error. The weighting factor λ balances their contributions. The error $\tilde{\epsilon}^2$ is defined as MSE for regression tasks (this apply for reconstruction error) or Cross Entropy for classification tasks. A similar loss is used for output uncertainty estimation. In parallel, we enhance the estimated output uncertainty by quantifying the uncertainty propagated from the reconstructed input, utilizing Error Propagation through the frozen pretrained network, as detailed in Section 2.3.

2.3 ERROR PROPAGATION THROUGH DEEP NETWORKS

While the classifier head quantifies output uncertainty from the stochastic nature of pretrained frameworks, a strategy is still required to account for uncertainty introduced by reconstructed inputs. Drawing from the Error Propagation formula Arras (1998); Tellinghuisen (2001), a fundamental principle in scientific measurement and data analysis used to quantify how input uncertainties affect derived quantities, we establish the following key result:

Proposition 2.2. *Let $\omega(\{Z^i\}_{i \in \mathcal{I}}, \{\tilde{Z}^j\}_{j \in \mathcal{J}})$ be the pretrained model in SURE, where \mathcal{I} and \mathcal{J} represent the sets of indices for which Z^i is available or unavailable, respectively. If each reconstructed modality \tilde{Z}^i has associated uncertainty $\tilde{\sigma}_{\tilde{Z}^i}^2$, then the total uncertainty propagated from reconstructed inputs is:*

$$\tilde{\sigma}_{input}^2 \approx \sum_{i \in \mathcal{J}} \left(\frac{\partial \omega}{\partial \tilde{Z}_i} \right)^2 \tilde{\sigma}_{\tilde{Z}_i}^2. \quad (8)$$

Derivation. The total uncertainty in a function $f(A_1, A_2, \dots, A_n)$ with n variables, each attached with uncertainty $\sigma_{A_i}^2$ ($i = 1, \dots, n$), is given by σ_f^2 and follows:

$$\sigma_f^2 \approx \sum_{i=1}^n \left(\frac{\partial f}{\partial A_i} \right)^2 \sigma_{A_i}^2, \quad (9)$$

Applying this to SURE model:

- The prediction function $\omega(\cdot)$ depends on both available inputs Z^i and reconstructed inputs \tilde{Z}_i .
- Disregard the uncertainty of available modalities, the uncertainty in reconstructed inputs \tilde{Z}_i propagates to the final output via its partial derivative.

Thus, we obtain the result in Proposition 2.2. \square

Combining $\tilde{\sigma}_{input}^2$ with the uncertainty stem from $\omega(\cdot)$ stochastic nature, denoted by $\tilde{\sigma}_\omega$ (quantified at SURE’s classifier head), we achieve the final output uncertainty:

$$\tilde{\sigma}_Y^2 = \tilde{\sigma}_{input}^2 + \tilde{\sigma}_\omega^2. \quad (10)$$

This combination follows the Pythagorean theorem for variances, which assumes the aggregated output uncertainty are caused by individual sources Dieck (2007): *input-induced uncertainty* (from missing modalities) and *model-intrinsic uncertainty* (from network stochasticity). Lastly, $\tilde{\sigma}_Y^2$ is learnt to reflect prediction error via \mathcal{L}_{PCC} discussed in Section 2.2.

Training process. In the first phase, reconstruction modules are trained with \mathcal{L}_{rec} using one modality as ground truth and others as input. In the second phase, reconstruction modules are frozen, and the classifier head is trained with \mathcal{L}_{PCC} and $\mathcal{L}_{downstream}$. Detailed training steps are in Algorithm 1 (Appendix A.2.3).

3 EXPERIMENTS

3.1 DATASETS AND METRICS

We integrate SURE into three pretrained multimodal frameworks and adapt them to smaller-scale datasets with missing modalities during training and evaluation. Detailed integration settings are provided in Appendix A.2.4.

Sentiment Analysis. For this task, we use MMML Wu et al. (2024), a state-of-the-art architecture pretrained on CMU-MOSEI Zadeh et al. (2018), and fine-tune it on CMU-MOSI Zadeh et al. (2016) with missing modalities.

Book Genre Classification. SURE is coupled with MMBT Kiela et al. (2019), pretrained on MM-IMDB Arevalo et al. (2020), and fine-tune it for book genre classification with text and image data from Haque et al. (2022).

Human Action Recognition. We use the HAMLET framework Islam & Iqbal (2020), pretrained on MMAct Kong et al. (2019), and fine-tune it on UTD-MHAD Chen et al. (2015) with missing modalities.

Uncertainty quality is evaluated using Uncertainty Calibration Error (UCE) Guo et al. (2017) and Pearson Correlation Coefficient (PCC) Upadhyay et al. (2022), which measure alignment between predictive error and uncertainty.

3.2 BASELINES AND EXPERIMENT DETAILS

For main comparison, we include reconstruction methods (ActionMAE Woo et al. (2023), DiCMoR Wang et al. (2023), IMDer Wang et al. (2024)) and uncertainty estimation methods (Gaussian Maximum Likelihood Kendall & Gal (2017b); Wang et al. (2019a), Monte Carlo Dropout Maddox et al. (2019); Laves et al. (2019); Srivastava et al. (2014), and Ensemble Learning Lakshminarayanan et al. (2017)). Baselines use the same pretrained models as SURE, and uncertainty methods are tested with a deterministic SURE* variant using MSE loss instead of \mathcal{L}_{rec} . Training datasets mask 50% of each modality’s samples, with distinct masks across modalities. Additional baselines and results are discussed in Appendix A.4.

Table 1: Results of different approaches on CMU-MOSI Dataset.

Model	MAE			Corr			F1			Acc			Reconstruct Uncertainty			Output Uncertainty		
	T(ext)	A(audio)	F(full)	T	A	F	T	A	F	T	A	F	T	A	T	A	F	
<i>Modality Reconstruction Techniques:</i>																		
ActionMAE	1.106	2.146	1.005	0.506	0.155	0.517	0.717	0.57	0.719	0.724	0.423	0.725	-	-	-	-	-	
DiCMoR	0.811	1.227	1.106	0.783	0.427	0.537	0.854	0.57	0.65	0.856	0.585	0.654	-	-	-	-	-	
IMDer	0.707	1.237	1.106	0.797	0.438	0.544	0.846	0.524	0.62	0.846	0.564	0.634	-	-	-	-	-	
<i>Uncertainty Estimation Techniques:</i>																		
SURE + Gaussian MLE	0.589	1.133	0.581	0.866	0.53	0.871	0.88	0.676	0.885	0.879	0.678	0.882	0.103	0.013	0.067	0.032	0.059	
SURE + MC DropOut	0.63	1.153	0.622	0.858	0.556	0.865	0.877	0.686	0.899	0.876	0.684	0.9	0.047	0.008	0.013	0.009	0.13	
SURE + DeepEnsemble	0.592	1.071	0.582	0.868	0.58	0.871	0.886	0.714	0.889	0.885	0.716	0.888	0.062	0.031	0.024	0.074	0.082	
SURE	0.602	1.148	0.583	0.865	0.557	0.869	0.896	0.685	0.891	0.894	0.684	0.89	0.739	0.732	0.381	0.18	0.485	

3.3 MAIN RESULTS

Results show pipeline performance with unimodal or full inputs, averaged over three runs. Best and second-best metrics are highlighted in **red** and **blue**, respectively.

Sentiment Analysis. The results for the CMU-MOSI dataset are summarized in Table 1. SURE and its variations consistently outperform recent reconstruction techniques, highlighting their effectiveness in handling missing modalities. SURE’s ability to reconstruct missing data on the fly during training allows every sample to be fully utilized, leading to improved final outputs. Among the modalities, audio appears to be less effective for the downstream task. All methods perform better when text is available compared to when only audio is used, and uncertainty estimation also declines when relying solely on audio.

Table 2: Results of different approaches on Book Dataset.

Model	F1			Acc			Reconstruct Uncertainty Corr		Output Uncertainty Corr			
	T(ext)	I(image)	F(ull)	T	I	F	T	I	T	I	F	
<i>Modality Reconstruction Techniques:</i>												
ActionMAE	0.277	0.271	0.35	0.186	0.166	0.311	-	-	-	-	-	-
DiCMoR	0.202	0.465	0.467	0.152	0.452	0.454	-	-	-	-	-	-
IMDer	0.204	0.376	0.374	0.155	0.368	0.367	-	-	-	-	-	-
<i>Uncertainty Estimation Techniques:</i>												
SURE + Gaussian MLE	0.676	0.238	0.685	0.665	0.233	0.672	0.137	0.233	0.358	0.349	0.468	
SURE + MC DropOut	0.653	0.491	0.669	0.65	0.466	0.658	0.243	0.334	0.174	0.186	0.41	
SURE + DeepEnsemble	0.682	0.327	0.684	0.673	0.31	0.673	0.128	0.135	0.144	0.214	0.227	
SURE	0.683	0.413	0.696	0.671	0.401	0.688	0.637	0.833	0.373	0.481	0.474	

Book Genre Classification. Similar to the sentiment analysis task, SURE outperforms recent reconstruction techniques in this classification task (Table 2), showing a stronger correlation between uncertainty and error for both reconstruction and downstream tasks. In the Book Dataset, the text modality proves to be highly effective for the downstream task, but it contributes less to uncertainty estimation for both reconstruction and downstream tasks.

Human Action Recognition. As suggested in Table 3, SURE consistently delivers the best performance on downstream tasks across all scenarios. Output uncertainty most closely reflects actual error when the Watch Accel modality is available. However, we observe that a modality effective for downstream task performance may not always contribute equally to uncertainty estimation. This is likely due to the independent nature of error distributions across different modality combinations, which leads to a divergence between downstream task performance and uncertainty estimation. Extended report with every input modalities combination is presented in Appendix A.4.1.

Table 3: Results of different approaches on UTD-MHAD Dataset.

Model	F1				Acc				Reconstruct Uncertainty Corr			Output Uncertainty Corr				
	V(ideo)	A(ccel)	G(yro)	F(ull)	V	A	G	F	V	A	G	V	A	G	F	
<i>Modality Reconstruction Techniques:</i>																
ActionMAE	0.044	0.204	0.303	0.531	0.059	0.231	0.311	0.537	-	-	-	-	-	-	-	
DiCMoR	0.069	0.473	0.52	0.653	0.033	0.408	0.472	0.636	-	-	-	-	-	-	-	
IMDer	0.089	0.157	0.141	0.687	0.069	0.158	0.145	0.689	-	-	-	-	-	-	-	
<i>Uncertainty Estimation Techniques:</i>																
SURE + Gaussian MLE	0.116	0.433	0.468	0.693	0.074	0.381	0.387	0.651	0.166	0.115	0.056	0.122	0.476	0.147	0.292	
SURE + MC DropOut	0.156	0.473	0.595	0.739	0.09	0.404	0.571	0.718	0.122	0.135	0.171	0.136	0.486	0.223	0.512	
SURE + DeepEnsemble	0.25	0.468	0.593	0.737	0.207	0.453	0.604	0.735	0.249	0.175	0.122	0.126	0.421	0.436	0.481	
SURE	0.161	0.462	0.607	0.739	0.121	0.431	0.59	0.74	0.878	0.837	0.863	0.226	0.53	0.306	0.568	

Summary. Compared to other methods, our \mathcal{L}_{PCC} loss avoids strict magnitude constraints, enabling efficient uncertainty learning and accurate error capture from inputs and model stochasticity. Metrics show strong uncertainty-error correlation in reconstruction and downstream tasks, validating SURE’s effectiveness.

4 ANALYSES

4.1 ABLATION STUDY.

Settings. We analyze the impact of various modules on SURE’s performance in both uncertainty estimation and downstream tasks. This analysis includes testing several ablated versions of SURE:

- (1a) **Remove $r^i(\cdot)$ modules:** Ignore incomplete samples during training.
- (1b) **Rule-based imputation:** Replace missing modalities with zeros.
- (2a) **Remove uncertainty estimation:** Train $r^i(\cdot)$ with MSE only, no uncertainty estimation.

Table 4: Results of different SURE’s variations of SURE on UTD-MHAD Dataset.

	Model	F1	Acc	Reconstruct Uncertainty Corr	Output Uncertainty Corr
Reconstruct Ablation	(1a) Full	0.151	0.098	-	0.124
	Video	0.095	0.094	-	0.128
	Accel	0.059	0.081	-	0.322
	Gyro	0.408	0.413	-	0.122
	Full	0.519	0.525	-	0.524
Uncertainty Est. Ablation	(2a) Video	0.173	0.117	-	-
	Accel	0.479	0.427	-	-
	Gyro	0.589	0.571	-	-
	Full	0.736	0.727	-	-
	(2b) Video	0.15	0.113	-	0.159
Pretraining Ablation	Accel	0.456	0.489	-	0.489
	Gyro	0.512	0.462	-	0.237
	Full	0.637	0.593	-	0.511
	(3) Video	0.031	0.005	0.684	0.026
	Accel	0.226	0.237	0.675	0.441
SURE	Gyro	0.434	0.418	0.68	0.463
	Full	0.615	0.618	-	0.472
	Video	0.161	0.121	0.878	0.226
SURE	Accel	0.462	0.431	0.837	0.53
	Gyro	0.607	0.59	0.863	0.306
	Full	0.739	0.74	-	0.568

(2b) **Remove reconstruction uncertainty:** Train $r^i(\cdot)$ with MSE; omit error propagation logic.

(3) **Remove pretrained weights:** Reinitialize and train backbone frameworks from scratch.

Results. We present the performance of all SURE variations on the UTD-MHAD dataset in Table 4. Overall, each ablation negatively impacts SURE’s performance in its respective tasks. Specifically, ignoring missing modalities (1a) or using simple rule-based imputation (1b) significantly reduces downstream task performance, as incomplete yet labeled data remains underutilized and pretrained frameworks is not effectively leveraged. Additionally, while removing uncertainty estimation logic has a negligible effect on the final task result (2a, 2b), this cause an inability to quantify output uncertainty effectively, ruin our initial effort in producing reliable predictions. Lastly, the results from variation (3) reinforce our motivation: utilizing pretrained weights is far more efficient and beneficial, especially for smaller datasets involving similar tasks.

4.2 ANALYSES FOR ESTIMATED UNCERTAINTY.

Convergence Analysis. We visualize the correlation between estimated uncertainties and prediction errors across all training epochs in Figure 4. Compared to the Negative Log-Likelihood Loss (NLL), \mathcal{L}_{PCC} demonstrates superior performance in both convergence speed and final estimation accuracy. Additionally, the shape of the NLL curve suggests instability, as the correlation trend declines after reaching its peak. Although there are fluctuations, our loss maintains an overall upward trend, eventually stabilizing in the final epochs. This experimental results are highly in accordant with our theoretical analysis of convergence points for NLL loss and our proposed loss (Appendix A.2.1).

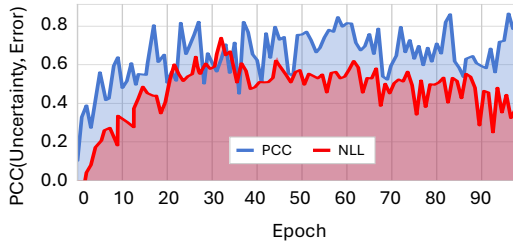
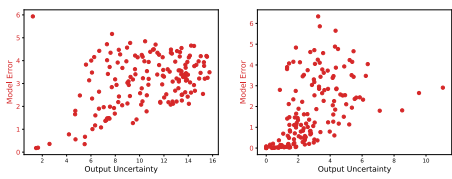


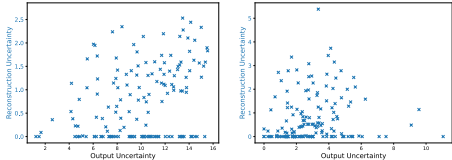
Figure 4: Correlation of estimated uncertainty with prediction error on UTD-MHAD dataset.

Reconstruction and Output Uncertainty Analysis. To better understand the relationship between prediction error, reconstruction uncertainty, and output uncertainty, we visualize these three quanti-



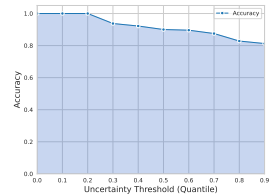
(a) Mod. 0 is missing (b) Mod. 1 is missing (c) Mod. 2 is missing

Figure 5: Relationship between estimated output uncertainty and output error on UTD-MHAD test dataset.

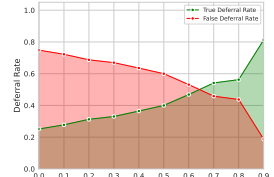


(a) Mod. 0 is missing (b) Mod. 1 is missing (c) Mod. 2 is missing

Figure 6: Relationship between estimated output uncertainty and reconstruction uncertainty on UTD-MHAD test dataset.



(a) Accuracy-Uncertainty



(b) TDR/FDR-Uncertainty

Figure 7: Decision Making Process with Uncertainty on UTD-MHAD Dataset.

ties across all test samples in the UTD-MHAD dataset, with different modalities combinations where each modality is missing. Ideally, the points should cluster along the bottom-left to top-right diagonal, indicating perfect correlation. With SURE, we observe high efficiency in estimating uncertainty for samples with large prediction errors, which aligns with its intended use as an indicator for potentially error-prone predictions (Figure 5). Notably, when output uncertainties are high, reconstruction uncertainties tend to be elevated as well (Figure 6), suggesting that uncertainties arising from the reconstruction process play a significant role in the overall uncertainty estimation. However, the visualization also indicates a tendency toward overestimating both reconstruction and output uncertainties, highlighting an area for potential improvement in future research.

4.3 APPLICATION: UNCERTAINTY-INFORMED DECISION MAKING WITH SURE

Settings. To demonstrate the impact of SURE’s uncertainty quantification on decision-making, we simulate this process using a human action recognition task with the UTD-MHAD dataset. SURE is trained with similar settings to those used in the main experiment (Table 3). After training, we use the uncertainty estimates to determine whether the model is confident enough to make a final decision or if it should defer the decision for manual inspection. Different uncertainty thresholds are set based on output uncertainty values from the test dataset. For each threshold, predictions with uncertainty higher than the threshold are deferred, and we record **Accuracy**, **True Deferral Rate**, and **False Deferral Rate** (representing the rate of correctly and incorrectly deferred samples) across all test samples.

Results. Figure 7a shows that as more uncertain predictions are deferred, the remaining predictions become more challenging, resulting in a decline in accuracy. This suggests that while the deferral strategy successfully excludes uncertain predictions, it also leaves a set of samples that are inherently harder to predict accurately. Additionally, Figure 7b demonstrates that as the uncertainty threshold increases, the true deferral rate rises, while the false deferral rate falls. This indicates that the model effectively identifies uncertain predictions (leading to more true deferrals) while reducing unnecessary deferrals. The point at which the true deferral rate surpasses the false deferral rate represents an optimal balance, maximizing decision quality and minimizing unwarranted deferrals. Combining the extended decision-making process under missing modality conditions (as presented in Appendix A.4.3), this analysis indicates that SURE’s estimated uncertainty is a reliable indicator for ensuring high prediction quality.

5 CONCLUSION

Contributions. This work introduces SURE (Scalable Uncertainty and Reconstruction Estimation), which leverages pretrained multimodal frameworks for small datasets with missing modalities using latent space reconstruction. SURE integrates uncertainty estimation via a Pearson Correlation-based loss and error propagation, ensuring reliable predictions and adaptability across tasks and networks. It achieves state-of-the-art results in both downstream performance and uncertainty estimation.

Limitations. In developing SURE, we observed that certain modalities dominate the reconstruction process, making it easier to predict missing ones but causing significant performance drops when unavailable. This imbalance, unexplored in the current SURE framework, may limit the development of robust reconstruction modules and presents a valuable direction for future work.

REFERENCES

John Arevalo, Thamar Solorio, Manuel Montes-y Gómez, and Fabio A. González. Gated multimodal networks. *Neural Comput. Appl.*, 32(14):10209–10228, July 2020. ISSN 0941-0643. doi: 10.1007/s00521-019-04559-1. URL <https://doi.org/10.1007/s00521-019-04559-1>.

Kai O Arras. An introduction to error propagation: derivation, meaning and examples of equation $cy = fx$ cx fxt . Technical report, ETH Zurich, 1998.

Murat Seckin Ayhan and Philipp Berens. Test-time data augmentation for estimation of heteroscedastic aleatoric uncertainty in deep neural networks. In *Medical Imaging with Deep Learning*, 2018.

Roman Bachmann, David Mizrahi, Andrei Atanov, and Amir Zamir. Multimae: Multi-modal multi-task masked autoencoders. In *European Conference on Computer Vision*, pp. 348–367. Springer, 2022.

Chen Chen, Roozbeh Jafari, and Nasser Kehtarnavaz. Utd-mhad: A multimodal dataset for human action recognition utilizing a depth camera and a wearable inertial sensor. In *2015 IEEE International conference on image processing (ICIP)*, pp. 168–172. IEEE, 2015.

Erik Daxberger, Agustinus Kristiadi, Alexander Immer, Runa Eschenhagen, Matthias Bauer, and Philipp Hennig. Laplace redux-effortless bayesian deep learning. *Advances in Neural Information Processing Systems*, 34:20089–20103, 2021.

Jacob Devlin. Bert: Pre-training of deep bidirectional transformers for language understanding. *arXiv preprint arXiv:1810.04805*, 2018.

Ronald H Dieck. *Measurement uncertainty: methods and applications*. ISA, 2007.

Runa Eschenhagen, Erik Daxberger, Philipp Hennig, and Agustinus Kristiadi. Mixtures of laplace approximations for improved post-hoc uncertainty in deep learning. *arXiv preprint arXiv:2111.03577*, 2021.

Christoph Feichtenhofer, Yanghao Li, Kaiming He, et al. Masked autoencoders as spatiotemporal learners. *Advances in neural information processing systems*, 35:35946–35958, 2022.

Huan Fu, Mingming Gong, Chaohui Wang, Kayhan Batmanghelich, and Dacheng Tao. Deep ordinal regression network for monocular depth estimation. In *Proceedings of the IEEE conference on computer vision and pattern recognition*, pp. 2002–2011, 2018.

Jakob Gawlikowski, Cedrique Rovile Njieutcheu Tassi, Mohsin Ali, Jongseok Lee, Matthias Humt, Jianxiang Feng, Anna Kruspe, Rudolph Triebel, Peter Jung, Ribana Roscher, et al. A survey of uncertainty in deep neural networks. *Artificial Intelligence Review*, 56(Suppl 1):1513–1589, 2023.

Chuan Guo, Geoff Pleiss, Yu Sun, and Kilian Q Weinberger. On calibration of modern neural networks. In *International conference on machine learning*, pp. 1321–1330. PMLR, 2017.

Zirun Guo, Tao Jin, and Zhou Zhao. Multimodal prompt learning with missing modalities for sentiment analysis and emotion recognition. *arXiv preprint arXiv:2407.05374*, 2024.

Emdadul Haque, Md Faraz Kabir Khan, Mohammad Imrul Jubair, Jarin Anjum, and Abrar Zahir Niloy. Book cover synthesis from the summary. In *2022 IEEE/ACS 19th International Conference on Computer Systems and Applications (AICCSA)*, pp. 1–6. IEEE, 2022.

Kaiming He, Xiangyu Zhang, Shaoqing Ren, and Jian Sun. Deep residual learning for image recognition. In *Proceedings of the IEEE conference on computer vision and pattern recognition*, pp. 770–778, 2016.

Yu Huang, Chenzhuang Du, Zihui Xue, Xuanyao Chen, Hang Zhao, and Longbo Huang. What makes multi-modal learning better than single (provably). *Advances in Neural Information Processing Systems*, 34:10944–10956, 2021.

Md Mofijul Islam and Tariq Iqbal. Hamlet: A hierarchical multimodal attention-based human activity recognition algorithm. In *2020 IEEE/RSJ International Conference on Intelligent Robots and Systems (IROS)*, pp. 10285–10292. IEEE, 2020.

Jaehyuk Jang, Yooseung Wang, and Changick Kim. Towards robust multimodal prompting with missing modalities. In *ICASSP 2024-2024 IEEE International Conference on Acoustics, Speech and Signal Processing (ICASSP)*, pp. 8070–8074. IEEE, 2024.

Alex Kendall and Yarin Gal. What uncertainties do we need in bayesian deep learning for computer vision? In I. Guyon, U. Von Luxburg, S. Bengio, H. Wallach, R. Fergus, S. Vishwanathan, and R. Garnett (eds.), *Advances in Neural Information Processing Systems*, volume 30. Curran Associates, Inc., 2017a. URL https://proceedings.neurips.cc/paper_files/paper/2017/file/2650d6089a6d640c5e85b2b88265dc2b-Paper.pdf.

Alex Kendall and Yarin Gal. What uncertainties do we need in bayesian deep learning for computer vision? *Advances in neural information processing systems*, 30, 2017b.

Alex Kendall and Yarin Gal. What uncertainties do we need in bayesian deep learning for computer vision? *Advances in neural information processing systems*, 30, 2017c.

Douwe Kiela, Suvrat Bhooshan, Hamed Firooz, Ethan Perez, and Davide Testuggine. Supervised multimodal bitransformers for classifying images and text. *arXiv preprint arXiv:1909.02950*, 2019.

Quan Kong, Ziming Wu, Ziwei Deng, Martin Klinkigt, Bin Tong, and Tomokazu Murakami. Mmact: A large-scale dataset for cross modal human action understanding. In *The IEEE International Conference on Computer Vision (ICCV)*, October 2019.

Balaji Lakshminarayanan, Alexander Pritzel, and Charles Blundell. Simple and scalable predictive uncertainty estimation using deep ensembles. *Advances in neural information processing systems*, 30, 2017.

Max-Heinrich Laves, Sontje Ihler, Karl-Philipp Kortmann, and Tobias Ortmaier. Well-calibrated model uncertainty with temperature scaling for dropout variational inference. *arXiv preprint arXiv:1909.13550*, 2019.

Changhee Lee and Mihaela Van der Schaar. A variational information bottleneck approach to multi-omics data integration. In *International Conference on Artificial Intelligence and Statistics*, pp. 1513–1521. PMLR, 2021.

Yi-Lun Lee, Yi-Hsuan Tsai, Wei-Chen Chiu, and Chen-Yu Lee. Multimodal prompting with missing modalities for visual recognition. In *Proceedings of the IEEE/CVF Conference on Computer Vision and Pattern Recognition*, pp. 14943–14952, 2023.

Mingcheng Li, Dingkang Yang, Yuxuan Lei, Shunli Wang, Shuaibing Wang, Liuzhen Su, Kun Yang, Yuzheng Wang, Mingyang Sun, and Lihua Zhang. A unified self-distillation framework for multimodal sentiment analysis with uncertain missing modalities. In *Proceedings of the AAAI Conference on Artificial Intelligence*, volume 38, pp. 10074–10082, 2024a.

Mingcheng Li, Dingkang Yang, Xiao Zhao, Shuaibing Wang, Yan Wang, Kun Yang, Mingyang Sun, Dongliang Kou, Ziyun Qian, and Lihua Zhang. Correlation-decoupled knowledge distillation for multimodal sentiment analysis with incomplete modalities. In *Proceedings of the IEEE/CVF Conference on Computer Vision and Pattern Recognition*, pp. 12458–12468, 2024b.

Zheng Lian, Lan Chen, Licai Sun, Bin Liu, and Jianhua Tao. Gcnet: Graph completion network for incomplete multimodal learning in conversation. *IEEE Transactions on pattern analysis and machine intelligence*, 45(7):8419–8432, 2023.

Mengmeng Ma, Jian Ren, Long Zhao, Sergey Tulyakov, Cathy Wu, and Xi Peng. Smil: Multimodal learning with severely missing modality. In *Proceedings of the AAAI Conference on Artificial Intelligence*, number 3 in 35, pp. 2302–2310, 2021.

Mengmeng Ma, Jian Ren, Long Zhao, Davide Testuggine, and Xi Peng. Are multimodal transformers robust to missing modality? In *Proceedings of the IEEE/CVF Conference on Computer Vision and Pattern Recognition*, pp. 18177–18186, 2022.

Wesley J Maddox, Pavel Izmailov, Timur Garipov, Dmitry P Vetrov, and Andrew Gordon Wilson. A simple baseline for bayesian uncertainty in deep learning. *Advances in neural information processing systems*, 32, 2019.

Petra Poklukar, Miguel Vasco, Hang Yin, Francisco S Melo, Ana Paiva, and Danica Kragic. Geometric multimodal contrastive representation learning. In *International Conference on Machine Learning*, pp. 17782–17800. PMLR, 2022.

Nitish Srivastava, Geoffrey Hinton, Alex Krizhevsky, Ilya Sutskever, and Ruslan Salakhutdinov. Dropout: a simple way to prevent neural networks from overfitting. *The journal of machine learning research*, 15(1):1929–1958, 2014.

Joel Tellinghuisen. Statistical error propagation. *The Journal of Physical Chemistry A*, 105(15):3917–3921, 2001.

Uddeshya Upadhyay, Shyamgopal Karthik, Yanbei Chen, Massimiliano Mancini, and Zeynep Akata. Bayescap: Bayesian identity cap for calibrated uncertainty in frozen neural networks. In *European Conference on Computer Vision*, pp. 299–317. Springer, 2022.

Zhexiong Wan, Yuxin Mao, Jing Zhang, and Yuchao Dai. Rpeflow: Multimodal fusion of rgb-pointcloud-event for joint optical flow and scene flow estimation. In *Proceedings of the IEEE/CVF International Conference on Computer Vision*, pp. 10030–10040, 2023.

Guotai Wang, Wenqi Li, Michael Aertsen, Jan Deprest, Sébastien Ourselin, and Tom Vercauteren. Aleatoric uncertainty estimation with test-time augmentation for medical image segmentation with convolutional neural networks. *Neurocomputing*, 338:34–45, 2019a.

Guotai Wang, Wenqi Li, Michael Aertsen, Jan Deprest, Sébastien Ourselin, and Tom Vercauteren. Aleatoric uncertainty estimation with test-time augmentation for medical image segmentation with convolutional neural networks. *Neurocomputing*, 338:34–45, 2019b.

Qi Wang, Liang Zhan, Paul Thompson, and Jiayu Zhou. Multimodal learning with incomplete modalities by knowledge distillation. In *Proceedings of the 26th ACM SIGKDD International Conference on Knowledge Discovery & Data Mining*, pp. 1828–1838, 2020.

Yuanzhi Wang, Zhen Cui, and Yong Li. Distribution-consistent modal recovering for incomplete multimodal learning. In *Proceedings of the IEEE/CVF International Conference on Computer Vision*, pp. 22025–22034, 2023.

Yuanzhi Wang, Yong Li, and Zhen Cui. Incomplete multimodality-diffused emotion recognition. *Advances in Neural Information Processing Systems*, 36, 2024.

Sangmin Woo, Sumin Lee, Yeonju Park, Muhammad Adi Nugroho, and Changick Kim. Towards good practices for missing modality robust action recognition. In *Proceedings of the AAAI Conference on Artificial Intelligence*, volume 37, pp. 2776–2784, 2023.

Mike Wu and Noah Goodman. Multimodal generative models for scalable weakly-supervised learning. *Advances in neural information processing systems*, 31, 2018.

Zehui Wu, Ziwei Gong, Jaywon Koo, and Julia Hirschberg. Multimodal multi-loss fusion network for sentiment analysis. In *Proceedings of the 2024 Conference of the North American Chapter of the Association for Computational Linguistics: Human Language Technologies (Volume 1: Long Papers)*, pp. 3588–3602, 2024.

Amir Zadeh, Rowan Zellers, Eli Pincus, and Louis-Philippe Morency. Multimodal sentiment intensity analysis in videos: Facial gestures and verbal messages. *IEEE Intelligent Systems*, 31(6):82–88, 2016.

AmirAli Bagher Zadeh, Paul Pu Liang, Soujanya Poria, Erik Cambria, and Louis-Philippe Morency. Multimodal language analysis in the wild: Cmu-mosei dataset and interpretable dynamic fusion graph. In *Proceedings of the 56th Annual Meeting of the Association for Computational Linguistics (Volume 1: Long Papers)*, pp. 2236–2246, 2018.

Daoming Zong and Shiliang Sun. Mcomet: Multimodal fusion transformer for physical audiovisual commonsense reasoning. In *Proceedings of the AAAI Conference on Artificial Intelligence*, volume 37, pp. 6621–6629, 2023.

A APPENDIX

A.1 RELATED WORKS

Multimodal missing modalities. Recent research has focused on developing models resilient to missing modalities Ma et al. (2021; 2022); Poklukar et al. (2022); Woo et al. (2023); Lee et al. (2023); Li et al. (2024b); Lian et al. (2023); Li et al. (2024a). Key directions include: (1) Contrastive loss-based methods that align latent spaces for cross-modal knowledge transfer Ma et al. (2022); Lee & Van der Schaar (2021); Wang et al. (2020); (2) Generative approaches, such as VAE-based models Wu & Goodman (2018) or latent space reconstruction Woo et al. (2023), to approximate missing inputs; and (3) Prompt-based techniques Lee et al. (2023); Guo et al. (2024); Jang et al. (2024) that use trainable prompts to adapt models to various combinations of missing modalities. In the first direction, representative methods like Smil Ma et al. (2021) employ Bayesian meta-learning to approximate latent features for incomplete data, while GMC Poklukar et al. (2022) ensures geometric alignment in multimodal representations, allowing unimodal data to substitute for missing modalities. For the second direction, ActionMAE, inspired by the masked autoencoder framework Feichtenhofer et al. (2022); Bachmann et al. (2022), reconstructs latent representations of missing modalities by randomly dropping feature tokens and learning to predict them. In the third direction, Lee et al. Lee et al. (2023) propose missing-aware prompts that are integrated into pretrained multimodal transformers during training, enabling models to handle missing modalities effectively during evaluation. While these approaches show promise in specific scenarios, they often rely heavily on large-scale datasets and lack robust mechanisms for quantifying uncertainty in the presence of missing modalities. SURE addresses these gaps by leveraging pretrained models that require less data and providing a robust framework for estimating uncertainty in both reconstructed inputs and downstream predictions, enhancing reliability and interpretability.

Uncertainty Estimation. Recent methods for uncertainty estimation in predictions primarily rely on Bayesian models Lakshminarayanan et al. (2017); Kendall & Gal (2017c). However, while these models can estimate uncertainty, their predictive performance often lags behind other approaches. Some post-hoc works have explored using Laplace approximation to estimate uncertainty Daxberger et al. (2021); Eschenhagen et al. (2021), but these methods require computing the Hessian matrix, making them infeasible for high-dimensional problems Fu et al. (2018). Another direction involves test-time data augmentation Wang et al. (2019b); Ayhan & Berens (2018), where multiple outputs are perturbed to estimate uncertainty. However, this approach is sometimes poorly calibrated, which is critical for accurate uncertainty estimation Gawlikowski et al. (2023). SURE offers a more efficient alternative by estimating uncertainty without compromising predictive performance on downstream tasks. Unlike Laplace approximation, SURE avoids computational issues in high-dimensional spaces, and it does not rely on test-time perturbations, ensuring better-calibrated uncertainty estimates across diverse settings. Additionally, SURE imposes no assumptions on the output size, making it more flexible for a variety of applications.

A.2 SURE’s ADDITIONAL DETAILS

A.2.1 NEGATIVE LOG LIKELIHOOD LOSS FOR UNCERTAINTY ESTIMATION

Analysis for the convergence of $\mathcal{L}_{NLL}(\cdot, \cdot)$.

The detailed derivation of the gradient of \mathcal{L}_{NLL} with respect to prediction \tilde{y}_i is:

$$\frac{\partial \mathcal{L}_{NLL}(\tilde{y}, \tilde{\sigma}^2)}{\partial \tilde{y}_i} = \frac{\partial}{\partial \tilde{y}_i} \sum_{i=1}^N \frac{\tilde{\epsilon}_i^2}{2\tilde{\sigma}_i^2} + \frac{\log(\tilde{\sigma}_i^2)}{2} = \frac{\tilde{\epsilon}_i}{\tilde{\sigma}_i^2} = \frac{\tilde{y}_i - y_i}{\tilde{\sigma}_i^2}.$$

Solving $\frac{\partial \mathcal{L}_{NLL}(\tilde{y}, \tilde{\sigma}^2)}{\partial \tilde{y}_i} = 0$ give us the closed form solution $\tilde{y}_i^* = y_i$ (One can further verify sufficient condition $\frac{\partial^2 \mathcal{L}_{NLL}(\tilde{y}_i, \tilde{\sigma}_i^2)}{\partial \tilde{y}_i^2} = \frac{1}{\tilde{\sigma}_i^2} > 0$ hold true $\forall i$).

Similarly, gradient of \mathcal{L}_{NLL} with respect to $\tilde{\sigma}_i^2$ is:

$$\frac{\partial \mathcal{L}_{NLL}(\tilde{y}, \tilde{\sigma}^2)}{\partial \tilde{\sigma}_i^2} = \frac{\partial}{\partial \tilde{\sigma}_i^2} \sum_{i=1}^N \frac{\tilde{\epsilon}_i^2}{2\tilde{\sigma}_i^2} + \frac{\log(\tilde{\sigma}_i^2)}{2} = \frac{1}{2(\tilde{\sigma}_i^2)^2} (\tilde{\sigma}_i^2 - \tilde{\epsilon}_i^2).$$

Setting $\frac{\partial \mathcal{L}_{NLL}(\tilde{y}, \tilde{\sigma}^2)}{\partial \tilde{\sigma}_i^2} = 0$ yield $\tilde{\sigma}_i^{2*} = \tilde{\epsilon}_i^2$. Verifying the sufficient condition:

$$\frac{\partial^2 \mathcal{L}_{NLL}}{\partial (\tilde{\sigma}_i^2)^2} \Bigg|_{\tilde{\sigma}_i^2 = \tilde{\epsilon}_i^2} = \frac{1}{2} \left(-\frac{1}{(\tilde{\epsilon}_i^2)^2} + \frac{2\tilde{\epsilon}_i^2}{(\tilde{\epsilon}_i^2)^3} \right) = \frac{1}{2} \left(-\frac{1}{\tilde{\epsilon}_i^4} + \frac{2}{\tilde{\epsilon}_i^4} \right) = \frac{1}{2} \cdot \frac{1}{\tilde{\epsilon}_i^4} > 0$$

This test result indicates a local minimum at $\tilde{\sigma}_i^{2*} = \tilde{\epsilon}_i^2$.

The issue optimizing $\mathcal{L}_{NLL}(\tilde{y}, \tilde{\sigma}^2)$ come up when $\tilde{\epsilon}_i \rightarrow 0$, this pull the gradient $\frac{\partial \mathcal{L}_{NLL}(\tilde{y}, \tilde{\sigma}_i^2)}{\partial \tilde{\sigma}_i^2}$ to the form $\frac{0}{0}$, which is mathematically undefined. This pose a significant issue for gradient-based optimization algorithms like Gradient Descent and cause arbitrary potential issues (gradient vanishing/exploding, numerical under/overflow sensitive to small changes of $\tilde{\epsilon}^2$, etc).

Analysis for the convergence of $\mathcal{L}_{PCC}(\cdot, \cdot)$.

For this analysis, we focus on the convergence for finding optimal $\tilde{\sigma}_i^{2*}$ of $\mathcal{L}_{PCC}(\cdot, \cdot)$. With:

$$\mathcal{L}_{PCC}(\tilde{\sigma}^2, \tilde{\epsilon}^2) = 1 - r(\tilde{\sigma}^2, \tilde{\epsilon}^2);$$

$$r(\tilde{\sigma}^2, \tilde{\epsilon}^2) = \frac{\sum_{i=1}^N (\tilde{\sigma}_i^2 - \mu_{\sigma^2})(\tilde{\epsilon}_i^2 - \mu_{\epsilon^2})}{\sqrt{\sum_{i=1}^N (\tilde{\sigma}_i^2 - \mu_{\sigma^2})^2} \sqrt{\sum_{i=1}^N (\tilde{\epsilon}_i^2 - \mu_{\epsilon^2})^2}} := \frac{A}{B}.$$

We have:

$$\frac{\partial \mathcal{L}_{PCC}(\tilde{y}, \tilde{\sigma}^2)}{\partial \tilde{\sigma}_i^2} = -\frac{\partial r(\tilde{y}, \tilde{\sigma}^2)}{\partial \tilde{\sigma}_i^2} = -\frac{1}{B} \frac{\partial A}{\partial \tilde{\sigma}_i^2} + \frac{A}{B^2} \frac{\partial B}{\partial \tilde{\sigma}_i^2}.$$

$$\begin{aligned} \frac{\partial A}{\partial \tilde{\sigma}_i^2} &= \frac{\partial}{\partial \tilde{\sigma}_i^2} \sum_{j=1}^N (\tilde{\sigma}_j^2 - \mu_{\sigma^2})(\tilde{\epsilon}_j^2 - \mu_{\epsilon^2}) \\ &= \sum_{j=1}^N (\delta_{ij} - \frac{1}{N})(\tilde{\epsilon}_j^2 - \mu_{\epsilon^2}) \text{ (where } \delta_{ij} = 1 \text{ if } i = j \text{ else 0)} \\ &= \tilde{\epsilon}_i^2 - \mu_{\epsilon^2} \text{ (Since } \frac{1}{N} \sum_{j=1}^N \tilde{\epsilon}_j^2 = \mu_{\epsilon^2}). \end{aligned}$$

Also,

$$\frac{\partial B}{\partial \tilde{\sigma}_i^2} = \frac{\partial}{\partial \tilde{\sigma}_i^2} \sqrt{\sum_{j=1}^N (\tilde{\sigma}_j^2 - \mu_{\sigma^2})^2} \sqrt{\sum_{j=1}^N (\tilde{\epsilon}_j^2 - \mu_{\epsilon^2})^2}$$

Denoting $\sigma_{\tilde{\sigma}^2} := \sum_{j=1}^N (\tilde{\sigma}_j^2 - \mu_{\sigma^2})^2$, $\sigma_{\tilde{\epsilon}^2} := \sum_{j=1}^N (\tilde{\epsilon}_j^2 - \mu_{\epsilon^2})^2$, we have:

$$\begin{aligned} \frac{\partial B}{\partial \tilde{\sigma}_i^2} &= \sigma_{\tilde{\epsilon}^2} \frac{1}{2\sigma_{\tilde{\sigma}^2}} \frac{\partial}{\partial \tilde{\sigma}_i^2} \sum_{j=1}^N (\tilde{\sigma}_j^2 - \mu_{\sigma^2})^2 \\ &= \sigma_{\tilde{\epsilon}^2} \frac{1}{2\sigma_{\tilde{\sigma}^2}} \left[\sum_{j=1}^N 2(\tilde{\sigma}_j^2 - \mu_{\sigma^2})(\delta_{ij} - \frac{1}{N}) \right] \\ &= \sigma_{\tilde{\epsilon}^2} \frac{1}{2\sigma_{\tilde{\sigma}^2}} \left[2(\tilde{\sigma}_i^2 - \mu_{\sigma^2}) - \frac{2}{N} \sum_{j=1}^N (\tilde{\sigma}_j^2 - \mu_{\sigma^2}) \right] \\ &= \sigma_{\tilde{\epsilon}^2} \sigma_{\tilde{\sigma}^2} \frac{\tilde{\sigma}_i^2 - \mu_{\sigma^2}}{\sigma_{\tilde{\sigma}^2}} \end{aligned}$$

Assembling the results, we have:

$$\begin{aligned}
\frac{\partial \mathcal{L}_{PCC}(\tilde{y}, \tilde{\sigma}^2)}{\partial \tilde{\sigma}_i^2} &= -\frac{\partial r(\tilde{y}, \tilde{\sigma}^2)}{\partial \tilde{\sigma}_i^2} = -\frac{1}{B} \frac{\partial A}{\partial \tilde{\sigma}_i^2} + \frac{A}{B^2} \frac{\partial B}{\partial \tilde{\sigma}_i^2} \\
&= -\frac{\tilde{\epsilon}_i^2 - \mu_{\epsilon^2}}{\sigma_{\tilde{\epsilon}^2} \sigma_{\tilde{\sigma}^2}} + \frac{\tilde{\sigma}_i^2 - \mu_{\sigma^2}}{\sigma_{\tilde{\sigma}^2}^2} * \frac{\sum_{j=1}^N (\tilde{\sigma}_j^2 - \mu_{\sigma^2}) (\tilde{\epsilon}_j^2 - \mu_{\epsilon^2})}{\sigma_{\tilde{\epsilon}^2} \sigma_{\tilde{\sigma}^2}} \\
&= -\frac{\tilde{\epsilon}_i^2 - \mu_{\epsilon^2}}{\sigma_{\tilde{\epsilon}^2} \sigma_{\tilde{\sigma}^2}} + \frac{\tilde{\sigma}_i^2 - \mu_{\sigma^2}}{\sigma_{\tilde{\sigma}^2}^2} * r(\tilde{\sigma}^2, \tilde{\epsilon}^2) \\
&= \frac{1}{\sigma_{\tilde{\sigma}^2}} \left[\frac{\tilde{\sigma}_i^2 - \mu_{\sigma^2}}{\sigma_{\tilde{\sigma}^2}} * r(\tilde{\sigma}^2, \tilde{\epsilon}^2) - \frac{\tilde{\epsilon}_i^2 - \mu_{\epsilon^2}}{\sigma_{\tilde{\epsilon}^2}} \right] \\
&= \frac{1}{\sigma_{\tilde{\sigma}^2}} [\sigma_{\tilde{\sigma}^2} * r(\tilde{\sigma}^2, \tilde{\epsilon}^2) - \sigma_{\tilde{\epsilon}^2}].
\end{aligned}$$

This last result suggest the gradient $\frac{\partial \mathcal{L}_{PCC}(\tilde{y}, \tilde{\sigma}^2)}{\partial \tilde{\sigma}_i^2}$ involves all standardized variables, which are within a manageable numerical range, reducing the risk of numerical instability. In addition, there is no divisions by $\tilde{\sigma}_i^2$, hence stabilize the training process even in the event when $\tilde{\epsilon}_i^2 \rightarrow 0$.

A.2.2 RECONSTRUCTION MODULES.

SURE involves a set of reconstruction modules to best leverage the pretrained models' weights. Each reconstruction module is tailored for a specific modality, hence this reconstruction logic is linearly scale with the total number of modalities.

Design. While not mentioned in SURE logic, it should be noted that all z^j are first linearly projected into a shared latent space wherever needed, before passing to the reconstruction modules. This step involves a single matrix multiplication done per modality, and the learnable matrix is trained together with the reconstruction modules. With that, all $r^i(\cdot)$'s are working with the same input latent space, we unify the design of $r^i(\cdot)$'s to be identical across different modalities. Specifically, the design of reconstruction module $r^i(\cdot)$ is kept as simple as possible, with the major component as Fully Connected layers and ReLU activations as follow:

$$\begin{aligned}
r_{share}^i(z^j) &= FC(ReLU(FC(z^j))), \\
r_{\mu}^i(z^j) &= FC(ReLU(FC(ReLU(r_{share}^i(z^j)))), \\
r_{\sigma}^i(z^j) &= SoftPlus(FC(ReLU(FC(ReLU(r_{share}^i(z^j) || r_{\mu}^i(z^j))).
\end{aligned} \tag{11}$$

In Equation 11, $||$ denotes the concatenation operation, and $SoftPlus()$ activation is used to ensure the positiveness of returned uncertainty.

Complexity. Below, we analyze the complexity of the chosen reconstruction modules. Table 5 lists hyper-parameters involved in the analysis.

Table 5: $r^i(\cdot)$ related hyper-parameters

Notation	Description
M	number of modalities
L	number of FC layers (in total)
d_i	hidden dimension of i^{th} layer's output
d_0	input dimension

Time Complexity. Assume a single multiplication or summation operation can be performed in unit time ($\mathcal{O}(1)$). We have the calculation for number of operations in a forward pass as follows.

Within the i^{th} FC layer:

$$d_{i-1} * d_i + d_i,$$

Over L layers:

$$\sum_{i=1}^L d_{i-1} * d_i + d_i.$$

In our implementations, we choose the same dimensions for all hidden outputs (same $d = d_i \forall i = 1, \dots, L$), and there are M modules $r^i(\cdot)$. With this, the total number of operation is:

$$M \sum_{i=1}^L d_{i-1} * d_i + d_i = M * L * d * (d + 1) = \mathcal{O}(M * L * d^2)$$

By utilizing matrix product and GPU acceleration, d^2 operations can in fact be performed in $\mathcal{O}(1)$ time, make the whole time complexity for individual branches be $\mathcal{O}(M * L)$, which is linearly scaled with M .

Space Complexity. Regarding the space complexity, within i^{th} layer, beside the need for storing parameter matrix of size $(d_{i-1} + 1) \times d_i$, output after performing *ReLU* activation are also stored to later perform back-propagation. Hence, the total number of stored parameters is:

$$(d_{i-1} + 1) * d_i + d_i = (d_{i-1} + 2) * d_i.$$

Following similar derivation with L layers and M branches, replacing $d = d_i \forall i = 1, \dots, L$, we have the total space complexity is:

$$M * L * (d + 2) * d = \mathcal{O}(M * L * d^2).$$

Despite utilizing straightforward reconstruction procedure, SURE demonstrates effective reconstruction in the latent space while maintaining an overall additional time and space complexity linearly scaled with M - the number of all modalities and L - the number of FC layers (6 in our implementation including both reconstruction and uncertainty heads).

A.2.3 EXTENSION TO M MODALITIES.

For extension to M modalities, we train the reconstruction module using \mathcal{L}_{rec} . We use each of the available modalities as the ground-truth output and the rest available modalities as input to predict. In the second phase, we freeze all of the reconstruction modules and train the classifier head with $\mathcal{L}_{downstream}$. For each sample with missing modalities, we reconstruct them with remaining available ones, and perform simple average operation to obtain the final reconstruction. Algorithm 1 summarize the whole training process of SURE for $m \geq 2$ modalities.

A.2.4 ADDITIONAL IMPLEMENTATION DETAILS

SURE’s Implementation Details. In SURE, we reutilize pretrained multimodal frameworks chosen for specific tasks. The only replacement is the final layers producing prediction, since the classification task might involve different number of classes, and there is an additional output head for estimation of output uncertainty.

Sentiment Analysis. This task involves predicting the polarity of input data (e.g., video, transcript). We use MMML Wu et al. (2024) trained on the CMU-MOSEI dataset Zadeh et al. (2018) as the pretrained framework. SURE’s reconstruction modules are added right after the projection modules - *Text/Audio feature networks* in original paper’s language Wu et al. (2024). Their fusion network are kept intact to leverage most pretrained weights as possible. We replace the last fully connected layer - classifier with two layers - one for the final output and one for estimated output uncertainty.

Book genre classification. This task involves classifying book genres based on their titles, summaries (text), and covers (images). We integrate SURE with MMBT Kiela et al. (2019), a pretrained

Algorithm 1 SURE training process

Input:

- ▷ $\mathcal{D}_{train} = \{(\mathbf{x}_k^i); \mathbf{y}_k | i \in \mathcal{I}_k\}$ – set of indices for available modalities in sample $k^{th}\}$.
- ▷ $f^i(\cdot)$ - frozen pretrained projectors; $r^i(\cdot)$ - reconstruction modules ($i = 1, \dots, M$).
- ▷ $\omega(\cdot)$ - frozen pretrained fusion module; $g(\cdot)$ - classifier head.

Output:

- ▷ $r^*(\cdot)$ - Trained reconstruction modules; $g^*(\cdot)$ - Trained classifier head ($i = 1, \dots, M$).

<pre> 1: Initialize $r^i(\cdot)$'s and $g(\cdot)$ ▷ Train reconstruction modules 2: for mini-batch $\mathcal{B} \in \mathcal{D}_{train}$ do 3: $l_{rec} \leftarrow 0$; 4: for $i \in \{1, \dots, M\}$ do 5: $l_{rec}^i \leftarrow 0$; 6: for $j \in \{1, \dots, M\}; j \neq i$ do 7: $\mathbf{z}_k^i = f^i(\mathbf{x}_k^i)$ ($\forall k : i \in \mathcal{I}_k$); 8: $\tilde{\mathbf{z}}_k^i, \tilde{\sigma}_k^i \leftarrow r^i(\mathbf{z}_k^j)$ ($\forall k : i, j \in \mathcal{I}_k$); 9: $l_{rec}^i \leftarrow l_{rec}^i + \mathcal{L}_{rec}(\mathbf{z}_i; \mathbf{z}_j)$; 10: end for 11: $l_{rec} \leftarrow l_{rec} + l_{rec}^i$; 12: end for 13: Backprop with l_{rec}; 14: Optimizer step; 15: end for </pre>	<pre> 16: Freeze reconstructed modules $r^i(\cdot)$; ▷ Train classifier head 17: for mini-batch $\mathcal{B} \in \mathcal{D}_{train}$ do 18: $\mathbf{z}_k^i = f^i(\mathbf{x}_k^i)$ ($\forall i : i \in \mathcal{I}_k$); 19: For $\forall i, j; i \notin \mathcal{I}_k, j \in \mathcal{I}_k$: 20: $\tilde{\mathbf{z}}_{j-k}^i, \tilde{\sigma}_{j-k}^i = r^i(\mathbf{x}_k^j)$; 21: $\tilde{\mathbf{z}}_k^i = \text{average}(\tilde{\mathbf{z}}_{j-k}^i)$; 22: $\tilde{\sigma}_{\tilde{\mathbf{z}}_k^i}^2 = \text{average}(\tilde{\sigma}_{j-k}^i)$; 23: $\tilde{\mathbf{y}}_k, \tilde{\sigma}_{\omega-k} \leftarrow g(\omega(\mathbf{z}_k^i, \tilde{\mathbf{z}}_k^i))$ 24: $\tilde{\sigma}_{input-k} \leftarrow \sum_{i \notin \mathcal{I}_k} \left(\frac{\partial \omega}{\partial \tilde{\mathbf{z}}_k^i} \right)^2 \tilde{\sigma}_{\tilde{\mathbf{z}}_k^i}^2$; 25: $\tilde{\sigma}_{\tilde{\mathbf{y}}_k}^2 \leftarrow \tilde{\sigma}_{input-k} + \tilde{\sigma}_{\omega-k}$; 26: $l_{downstream} \leftarrow \mathcal{L}_{downstream}(\tilde{\mathbf{y}}_k; \mathbf{y}_k)$; 27: $l_{y-pcc} \leftarrow \mathcal{L}_{PCC}(\tilde{\sigma}_{\tilde{\mathbf{y}}_k}^2; l_{downstream})$; 28: Backprop with l_{y-pcc} and $l_{downstream}$; Optimizer step; 29: end for </pre>
--------------------------------------------------------------------------------------------------------------------------------------------------------------------------------------------------------------------------------------------------------------------------------------------------------------------------------------------------------------------------------------------------------------------------------------------------------------------------------------------------------------------------------------------------------------------------------------------------------------------------------------------------------------------------------------------------------------------------------------------------------------------------------------------------------------------------------------------------------------------------------------------------------------------------------------------------------------------------------------------	----------------------------------------------------------------------------------------------------------------------------------------------------------------------------------------------------------------------------------------------------------------------------------------------------------------------------------------------------------------------------------------------------------------------------------------------------------------------------------------------------------------------------------------------------------------------------------------------------------------------------------------------------------------------------------------------------------------------------------------------------------------------------------------------------------------------------------------------------------------------------------------------------------------------------------------------------------------------------------------------------------------------------------------------------------------------------------------------------------------------------------------------------------------------------------------------------------------------------------------------------------------------------------------------------------------------------------------------------------------------------------------------------------------------------------------------------------------------------------------------------------------------

framework on the MM-IMDB dataset Arevalo et al. (2020). MMBT is a bitransformer architecture, hence we consider the all the processing before positional embedding and segment embedding as the projection logic (refer to Kiela et al. (2019) for clearer architecture details), and add our reconstruction modules are inserted after this logic. The remaining transformer logic are considered fusion modules, and kept intact.

Human Action Recognition. This task involves identifying human actions based on recorded videos and sensor data. We use HAMLET framework Islam & Iqbal (2020), pretrained on the large-scale MMAAct dataset Kong et al. (2019) for this task. HAMLET define their projection modules as *Unimodal Feature Encoders* Islam & Iqbal (2020). SURE's reconstruction modules are included right after these encoders, while retain their original MAT module.

Baselines' Implementation Details. In our comparative evaluation, we incorporate several state-of-the-art approaches, each representing prominent strategies. The baselines are grouped into two categories, reflecting the key challenges addressed by SURE: (1) Reconstruction methods for missing modalities, and (2) Uncertainty estimation methods. The reconstruction techniques include Action-MAE Woo et al. (2023), DiCMoR Wang et al. (2023), and IMDer Wang et al. (2024). For uncertainty estimation, we evaluate against the Gaussian Maximum Likelihood method Kendall & Gal (2017b); Wang et al. (2019a), Monte Carlo Dropout Maddox et al. (2019); Laves et al. (2019); Srivastava et al. (2014), and Ensemble Learning Lakshminarayanan et al. (2017). The original codebases of all baseline implementations are used for best reproducibility.

For all baselines, we also reutilize pretrained multimodal frameworks chosen for specific tasks like the adoption with SURE. In addition, the hidden dimension used within Reconstruction-based baselines are also modified to be the same as those used within SURE for fair comparison.

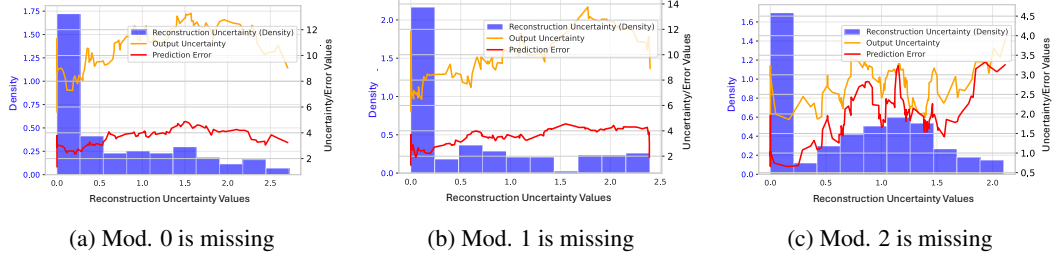


Figure 8: Inter-relationship between estimated output uncertainty, reconstruction uncertainty and output error on UTD-MHAD test dataset.

A.3 ENVIRONMENT SETTINGS

All implementations and experiments are performed on a single machine with the following hardware setup: a 6-core Intel Xeon CPU and two NVIDIA A100 GPUs for accelerated training.

Our codebase is primarily built using *PyTorch 2.0*, incorporating *Pytorch-AutoGrad* for deep learning model development and computations. We also use tools from *Scikit-learn*, *Pandas*, and *Matplotlib* to support various experimental functionalities. The original codebase for SURE will be released publicly upon publication.

A.4 ADDITIONAL EXPERIMENTS AND ANALYSES

A.4.1 EXTENDED MODALITIES MISSING SCENARIOS

In Table 6, we provide a comprehensive evaluation of different frameworks across all combinations of input modalities on the UTD-MHAD dataset. This table expands on the information presented in Table 3 in the main text. The reported reconstruction uncertainty for cases with more than one available modality is averaged over all missing modalities (e.g., given (Video + Accel) inputs, the reported reconstruction uncertainty represents the average value for Gyro reconstruction). The results show that SURE consistently delivers the best performance in most uncertainty estimation scenarios while maintaining competitive results for the downstream task, underscoring its robustness across different missing modality situations.

A.4.2 EXTEND ANALYSIS FOR INTER-RELATIONSHIP BETWEEN ESTIMATED UNCERTAINTIES AND ERROR.

We further analyze Figure 8 to explore the inter-relationship between prediction error, reconstruction uncertainty, and output uncertainty. This visualization includes all test samples from the UTD-MHAD dataset under different modality-missing scenarios, where each modality is systematically excluded. The histogram represents reconstruction uncertainty, while two line plots illustrate output uncertainty and prediction error.

Ideally, the two line plots should display an increasing trend, indicating a positive correlation with reconstruction uncertainty. Using SURE, such a trend is partially observed when modalities 0 and 1 are missing; however, it is less evident when modality 2 is missing. When combined with downstream performance for different input modality combinations, this experiment reveals two key insights:

- The Importance of Strong Modalities: Modality 2 (Gyro) plays a critical role in both downstream task performance and reconstructing other modalities. This suggests that stronger modalities are more effective in compensating for or reconstructing missing inputs to solve particular downstream tasks.
- Correlations Between Quantities: Output uncertainty is strongly correlated with prediction error, whereas reconstruction uncertainty shows a weaker correlation. This result aligns with our design: output uncertainty is directly trained to reflect prediction error, while reconstruction uncertainty may not be the primary source of error—model limitations and other factors can also contribute significantly.

Table 6: Results of different approaches on UTD-MHAD Dataset given every possible combination of input modalities.

Model	F1	Acc	Reconstruct	Output
			Uncertainty Corr	Uncertainty Corr
ActionMAE	Video	0.044	0.059	-
	Accel	0.204	0.231	-
	Gyro	0.303	0.311	-
	Video + Accel	0.034	0.085	-
	Video + Gyro	0.301	0.305	-
	Accel + Gyro	0.31	0.306	-
	Full	0.531	0.537	-
DiCMoR	Video	0.069	0.033	-
	Watch Accel	0.473	0.408	-
	Phone Gyro	0.52	0.472	-
	Video + Accel	0.524	0.449	-
	Video + Gyro	0.536	0.553	-
	Accel + Gyro	0.577	0.586	-
	Full	0.653	0.636	-
IMDer	Video	0.089	0.069	-
	Watch Accel	0.157	0.158	-
	Phone Gyro	0.141	0.145	-
	Video + Accel	0.152	0.152	-
	Video + Gyro	0.248	0.257	-
	Accel + Gyro	0.316	0.278	-
	Full	0.687	0.689	-
SURE + Gaussian MLE	Video	0.116	0.074	0.166
	Watch Accel	0.433	0.381	0.115
	Phone Gyro	0.468	0.387	0.056
	Video + Accel	0.432	0.443	0.104
	Video + Gyro	0.462	0.502	0.095
	Accel + Gyro	0.639	0.67	0.242
	Full	0.693	0.651	-
SURE + MC DropOut	Video	0.156	0.09	0.122
	Watch Accel	0.473	0.404	0.135
	Phone Gyro	0.595	0.571	0.171
	Video + Accel	0.452	0.52	0.186
	Video + Gyro	0.546	0.56	0.101
	Accel + Gyro	0.618	0.639	0.201
	Full	0.739	0.718	-
SURE + DeepEnsemble	Video	0.25	0.207	0.249
	Watch Accel	0.468	0.453	0.175
	Phone Gyro	0.593	0.604	0.122
	Video + Accel	0.652	0.662	0.092
	Video + Gyro	0.776	0.781	0.176
	Accel + Gyro	0.839	0.843	0.278
	Full	0.737	0.735	-
SURE	Video	0.161	0.121	0.878
	Watch Accel	0.462	0.431	0.837
	Phone Gyro	0.607	0.59	0.863
	Video + Accel	0.542	0.606	0.873
	Video + Gyro	0.609	0.637	0.862
	Accel + Gyro	0.679	0.706	0.455
	Full	0.739	0.74	-

These observations highlight the nuanced dynamics between uncertainties and error quantities produced with SURE.

A.4.3 EXTEND DECISION MAKING ANALYSIS

Building on the main text analysis, we simulate the decision-making process on the UTD-MHAD dataset under conditions where different modalities are missing (Figures 9, 10, 11). Each figure represents the inference scenarios when the Video, Accel, or Gyro modality is absent. Similar to the decision-making process with full modalities, incorporating uncertainty estimates in cases

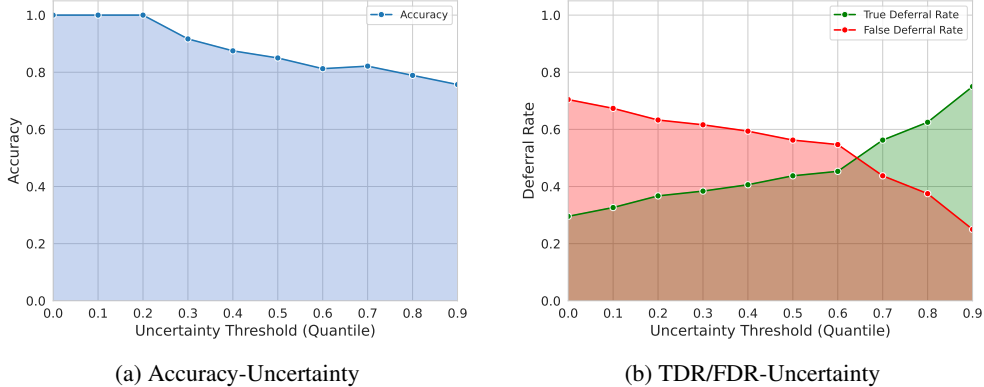


Figure 9: Decision Making with uncertainty when Video is missing

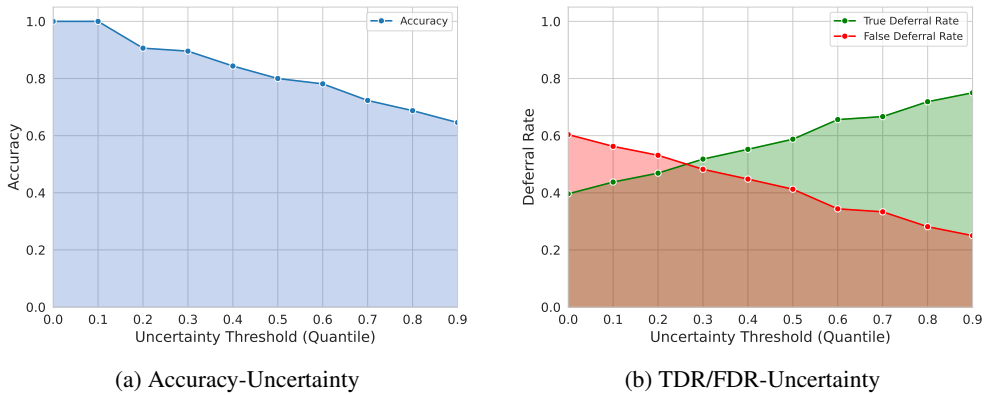


Figure 10: Decision Making with uncertainty when Accel is missing

with missing modalities continues to guide a reliable decision-making process by adjusting different uncertainty thresholds.

Lastly, for an aggregated perspective, the figure 12 shows the combined decision-making analysis on the UTD-MHAD dataset across different input modality combinations, with a deferral threshold set at the 0.65 quantile of output uncertainty. The green bars represent the true deferral rate, which indicates the proportion of incorrect predictions successfully deferred, while the red bars indicate the false deferral rate, representing the proportion of correct predictions unnecessarily deferred. The blue line shows the accuracy of the non-deferred predictions. From this visualization, the model effectively defers incorrect predictions when modality 0 is missing (true deferral rate ~ 0.91), but performance declines as more modalities are removed, with a notable drop for modality 2 (Gyro). False deferral rates remain low but vary slightly across scenarios at the chosen threshold (0.65 uncertainty quantile), suggesting that the optimal uncertainty threshold may differ depending on the input modality combination. Non-deferred prediction accuracy decreases significantly when critical modalities like modality 2 are missing, underscoring its importance for robust performance. While the deferral strategy effectively reduces errors, further optimization of uncertainty thresholds is required to adapt to varying input modalities.

A.4.4 ADDITIONAL COMPARISON WITH PROMPT-BASED TECHNIQUES

We further compare our SURE pipeline with two representative approaches that use prompt-based tuning techniques to address missing modalities Lee et al. (2023); Guo et al. (2024). Similar to our work, these approaches also leverage pretrained multimodal pipelines for efficient training. Their key innovation lies in introducing trainable prompts to indicate the presence of missing modalities.

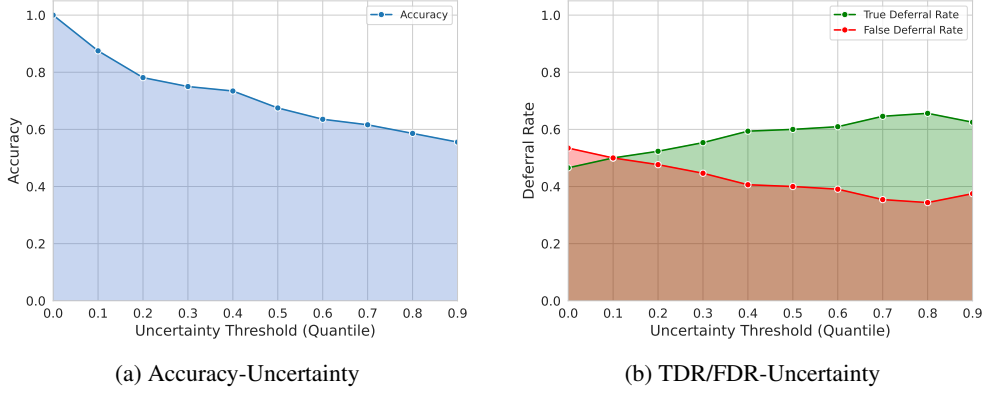


Figure 11: Decision Making with uncertainty when Gyro is missing



Figure 12: Decision making analysis with different input modalities combinations on UTD-MHAD dataset, with defer threshold set to be 0.65 quantile.

Setting. The chosen task for demonstration is Semantic Analysis task. In line with the CMU-MOSI experiment described in the main text, both frameworks are implemented using the MMML Wu et al. (2024) model, pretrained on the CMU-MOSEI dataset Zadeh et al. (2018). To ensure a fair comparison, all core modules from the original codebases of the two approaches are preserved to accurately replicate their performance. The training dataset is designed similarly to the main experiment, with 50% of modalities randomly masked and treated as missing.

Result. As shown in Table 7, SURE outperforms the two prompt-based approaches in handling missing modalities, achieving better downstream task performance. This advantage may stem from the limited number of learnable parameters introduced by these techniques, which likely constrain their ability to adapt effectively to scenarios with missing modalities.

Table 7: Additional results of different approaches on CMU-MOSI Dataset.

Model	MAE			Corr			F1			Acc		
	T(ext)	A(audio)	F(ull)	T	A	F	T	A	F	T	A	F
MPMM	0.683	1.197	0.668	0.83	0.495	0.834	0.87	0.69	0.874	0.871	0.689	0.875
MPLMM	0.624	1.166	0.607	0.838	0.509	0.842	0.865	0.697	0.879	0.865	0.694	0.879
SURE	0.602	1.148	0.583	0.865	0.557	0.869	0.896	0.685	0.891	0.894	0.684	0.89